Two sources of uncertainty in estimating tephra volumes from isopachs: perspectives and quantification

Qingyuan Yang[1,2,*,**] and Susanna F Jenkins[1,2]

[*]qingyuan.yang@ntu.edu.sg
[**]Now at the Department of Earth and Environmental Engineering, Columbia University, New York, USA
[1]Earth Observatory of Singapore, Singapore, Singapore
[2]Asian School of the Environment, Nanyang Technological University, Singapore, Singapore

December 27, 2022

Contents

Abstract

Calculating the volume of tephra erupted is important for estimating eruption intensity and magnitude. Traditionally, tephra volumes are estimated by integrating the area under curves fit to the square root of hand-drawn isopach areas. Previous studies have attempted to quantify the uncertainty in this approach, but not all sources of uncertainty have been well-analyzed or addressed. In this work, we study two such sources of uncertainty in estimating tephra volumes based on isopachs. The first source is model uncertainty. It occurs because no fitted curves perfectly describe the tephra thinning pattern, and the fitting is done based on log-transformed thickness and the square-root of isopach area. This model uncertainty is often omitted or considered compensated for or overridden by the presence other sources of uncertainty. The second source of uncertainty occurs because thickness must be extrapolated beyond the available data (i.e. beyond isopachs), which makes it impossible to validate the extrapolated thickness. It has been pointed out in a previous work, but remains unresolved. We demonstrate the importance of the two sources of uncertainty on a theoretical level. We use six isopach datasets with different features (e.g., spacing, coverage, and number of isopachs) to demonstrate their presence and the effect they could have on volume estimation. Measures to better represent the uncertainty are proposed and tested. For uncertainty arising from the model uncertainty, we propose: i) a better-informed and stricter way to report and evaluate goodness-of-fit, and ii) that uncertainty estimations be based on the envelope (or union thickness) defined by different well-fitted curves, rather than volumes estimated from individual curves. For the second source of uncertainty, we support reporting separately the volume portions that are interpolated between isopachs and those that are extrapolated, and we propose to test how sensitive the total volume is to variability in the extrapolated volume. The two sources of uncertainty should not be ignored as they could introduce additional bias, and lead to under- or over-estimated uncertainty in the volume estimate.

1 Introduction

Calculating the volume of tephra fall deposits is important for the study of explosive volcanic eruptions (Fierstein and Nathenson, 1992; Pyle, 1989). Its value is critical to the eruption VEI or magnitude assessment (Newhall and Self, 1982; Pyle, 2015), is tied to physical processes of eruptions, and helps to constrain other eruption source parameters (e.g., Mastin et al., 2009). Conventionally, tephra volume is estimated based on hand-drawn isopachs using the method proposed by Pyle (1989) and Fierstein and Nathenson (1992). Novel statistical and engineering methods have been proposed to construct isopachs, generate tephra thickness distributions and estimate tephra volumes (e.g., Engwell et al., 2015; Green et al., 2016; Yang and Bursik, 2016; White et al., 2017; Rougier et al., 2022). Studies have also identified and characterized different sources of uncertainty (e.g., those from field measurements and isopach construction) in tephra volume estimation, using methods such as Monte Carlo, Bootstrapping, and Bayes theorem (e.g., Engwell et al., 2013; Buckland et al., 2020; Rougier et al., 2022; Biass et al., 2019; Yang et al., 2021; Constantinescu et al., 2022). Despite the carefulness, strictness, and robustness in these studies, it is widely accepted that we should still interpret the estimated volume and quantified uncertainty with caution, because of the difficulty in objectively quantifying different sources of uncertainty (e.g., assigning appropriate value to quantify the measurement uncertainty). Despite the development of novel methods that do not use isopachs to estimate tephra volume (e.g. Engwell et al., 2013; Yang and Bursik, 2016; Rougier et al., 2022), the isopach-based method proposed by Pyle (1989) and Fierstein and Nathenson (1992) is still being widely used to estimate or validate new methods for tephra volume (e.g., Buckland et al., 2020; Prival et al., 2020; Takarada and Hoshizumi, 2020).

1.1 Motivation

The isopach-based method works by plotting the isopach data on the log(thickness) $-\sqrt{\text{isopach area}}$ plot, fitting curves to the data, and implementing integration based on the fitted curves (Pyle, 1989; Fierstein and Nathenson, 1992). Methods to quantify the tephra volume uncertainty using this method have been proposed and widely used (e.g., Daggitt et al., 2014; Biasse et al., 2014; Biass et al., 2019), but there is still one source of uncertainty and one question left unresolved with the method. The uncertainty occurs due to the fact that there is not a curve that always fits perfectly well to the data, which introduces model uncertainty to the volume estimate. This uncertainty is often omitted or considered compensated or overridden by other sources of uncertainty such as the uncertainty in constructing isopachs, while the uncertainty in constructing isopachs should be categorized as data uncertainty and thus distinguished from the model uncertainty.

The question left unanswered is proposed in Klawonn et al. (2014a), which suggested that the uncertainties for tephra volumes associated with interpolated thickness (i.e. those between isopachs) and extrapolated thickness (i.e. those within the thickest and outside of the thinnest isopach) will differ and should be treated separately. The two sources of uncertainty will be introduced with greater detail later in the text.

The model uncertainty and the unanswered question listed above should not be neglected in estimating tephra volumes when the isopach-based method is used. Different factors and processes contribute to the uncertainty in tephra volume estimation following a hierarchical order (Fig. 1a). Before the thickness was measured in the field, processes such as reworking would modify the primary tephra thickness. The measured thickness during field work is also subject to measurement uncertainty (Engwell et al., 2013; Kawabata et al., 2013; Green et al., 2016). To use the isopach-based method to estimate tephra volume, the construction of isopachs also introduces additional uncertainty after collecting the thickness observations (Engwell et al., 2013; Klawonn et al., 2014b). The two sources of uncertainty mentioned above and studied in this work are the last uncertainty sources introduced before the volume estimation, as they derive from the curve fitting process (which leads to the final volume estimation through integration). All sources of uncertainty listed above propagate in a way similar to the chain rule, and thus cannot be superimposed. If we ignore the last two sources of uncertainty, instead of inheriting the uncertainty from previous steps in the hierarchy and propagating their own uncertainty, they might dampen, exaggerate, or even distort the uncertainty inherited from previous steps, and introduce additional, irrelevant bias and uncertainty to the final volume estimate. A simple sketch in Fig. 1b shows the situation in which the estimated volume range does not cover the true tephra volume if the model uncertainty was omitted.

The above arguments demonstrate the importance of the two sources of uncertainty on a theoretical level, but it is possible that their impacts on the volume estimate are relatively small, and can be overridden by other uncertainties. Whether it is the case depends on the specific isopach dataset and perspectives to view and interpret the two sources of uncertainty, which will be illustrated in the following text.

In this work, we study and demonstrate the presence of the two sources of uncertainty when the isopach-based method is used for tephra volume estimation, and propose measures and perspectives to address and interpret them. We first introduce the log(thickness) $-\sqrt{\text{isopach area}}$ plot method, datasets, and parameters used in this work. Then we demonstrate the presence of the two, and propose measures to address them. The main contributions of this work include: (1) explicitly pointing out the two sources of uncertainty and their importance and (2) the proposed measures to address and interpret the two sources of uncertainty.

They present a more accurate and more logically consistent way to capture and interpret the two sources of uncertainty when the isopach-based method is used.

Throughout this work, we assume that a set of isopachs, rather than individual thickness measurements, is available for each tephra deposit to be analyzed. We assume that all isopachs are uncertainty-free unless otherwise specified, namely they represent the *true* isopach areas of the studied deposits at the corresponding thicknesses. In other words, all misfit between the isopach data and fitted curves belongs to the model uncertainty that is of interest in this work. With these assumptions, we neglect uncertainties such as those from measuring tephra thickness in the field, the effect of post-eruption weathering, movement or compaction, and from constructing isopachs, and assume that they can be analyzed in other stages of the uncertainty quantification. These assumptions are necessary as otherwise we cannot exclude the impact of other uncertainties on our analysis. We also do not attempt to use our knowledge on the physics of tephra transport to constrain the thinning pattern of tephra deposits as is done in some previous works (e.g., Carey and Sparks, 1986; Bursik et al., 1992; Bonadonna et al., 1998; Koyaguchi and Ohno, 2001). This is independent from the two sources of uncertainty, and represents another uncertainty source that should be included in other stages of the uncertainty quantification. In this work, for a volume to be estimated (e.g., total tephra volume or the volume of a subset of a tephra deposit), we quantify the uncertainty as the difference between the maximum and minimum estimates, referred to here as volume variability.

2 Background

2.1 The isopach-based method

Pyle (1989) and Fierstein and Nathenson (1992) proposed that the volume (V) of tephra deposits can be calculated as:

$$V = \int_0^\infty T\,dA = \int_0^\infty T 2A^{1/2}\,dA^{1/2}, \tag{1}$$

where T is tephra thickness, and A is the isopach area. The tephra volume can be calculated using Eq. 1 if a relationship exists between T and $A^{1/2}$. The relationship can be determined by fitting certain curves to the isopach data. Three types of curves have been proposed so far for the fitting. The first one is the one-segment or multi-segment exponential functions proposed in Pyle (1989) and Fierstein and Nathenson (1992). The one-segment form is written as:

$$T = T_0 \exp(-kA^{1/2}), \tag{2}$$

where T_0 is the extrapolated thickness when $A = 0$, and $-k$ is the slope of the line on the log(thickness) $-$ $\sqrt{\text{isopach area}}$ plot. The multi-segment form, as its name suggests, is composed of two or more connected functions each defined by Eq. 2 with different intercepts and slopes on the log(thickness) $-$ $\sqrt{\text{isopach area}}$ plot. In particular, the two-segment form is defined by two extrapolated thicknesses (T_0 and T_1), two slopes on the log(thickness)$-$$\sqrt{\text{isopach area}}$ plot defining the different thinning rates (k and k_1), and a value defining where the two intersect ($A_{ip}^{1/2}$). The power-law relationship is proposed in Bonadonna and Houghton (2005), and can be written as:

$$T = T_{pl}(A^{1/2})^{-m}, \tag{3}$$

where T_{pl} is a constant, and m is the power-law coefficient. Bonadonna and Costa (2012) used Weibull function to describe the relationship between T and $A^{1/2}$:

$$T = \theta(\frac{A^{1/2}}{\lambda})^{n-2} \exp(-(\frac{A^{1/2}}{\lambda})^{n}), \tag{4}$$

where λ is a characteristic decay length scale denoting deposit thinning, θ corresponds to a thickness scale, and n is a shape parameter. By substituting Eqs. 2 - 4 and the segmented form of Eq. 2 each to Eq. 1, the total volume of tephra deposit can be integrated analytically. The corresponding parameters of the curves (Eqs. 2 - 4) are derived through curve fitting based on hand-drawn isopachs or isopachs from interoplation techniques. For the power-law function (Eq. 3), (both proximal and distal) limits need to be specified during integration to prevent the total volume from going to infinity (Bonadonna and Houghton, 2005). It is noted by Fierstein and Nathenson (1992) that we could change the limits in Eq. 1 from 0 to infinity to any other $\sqrt{\text{isopach area}}$ ranges, say isopachs A and B with areas A_a and A_b and thicknesses T_a and T_b. If we assume that tephra thins exponentially between $\sqrt{A_a}$ and $\sqrt{A_b}$, the tephra volume (V_{a-b}) between the two isopachs is written as (the equation below is from Eq. 13 of Fierstein and Nathenson, 1992):

$$V_{a-b} = \frac{2T_{0a-b}}{k_{a-b}^2}[(k_{a-b}A_a^{1/2} + 1)\exp(-k_{a-b}A_a^{1/2}) - (k_{a-b}A_b^{1/2} + 1)\exp(-k_{a-b}A_b^{1/2})], \tag{5}$$

where k_{a-b} and $\log(T_{0a-b})$ are the slope and intercept of the line defined by the two isopachs on the log(thickness) $-$ $\sqrt{\text{isopach area}}$ plot. With the help of the trapezoidal rule, we could use Eq. 5 to calculate the volume within any pair of isopachs for a certain fitted curve (Fig. 2a).

2.1.1 (N-1)-segment exponential curve

Another form of the multi-segment exponential function needs to be introduced as it will assist the analysis in this work. It simply extends the one or two exponential segments to (N-1) segments on the log(thickness) $-$ $\sqrt{\text{isopach area}}$ plot. Here N refers to the number of isopachs for the deposit. It has been adopted in previous studies before (e.g., Fierstein and Nathenson, 1992), but is not widely adopted in more recent studies. We refer to it as the $(N-1)$-segment exponential curve in this work. Each segment of this curve is defined by the straight line connected by a pair of neighboring isopach data on the the log(thickness) $-$ $\sqrt{\text{isopach area}}$ plot (Fierstein and Nathenson, 1992). For ranges from zero to the $\sqrt{\text{thickest isopach area}}$ and from the $\sqrt{\text{thinnest isopach area}}$ to infinity, the curve can be simply defined by extending the first and last segments. The (N-1)-segment exponential curve is unique because it is defined by the isopach data, and it does not require additional curve-fitting procedure.

2.2 Datasets

We use isopach datasets from six well-studied tephra deposits as examples in this work. The deposits are the tephras from the 1815 Tambora eruption (Kandlbauer and Sparks, 2014), Taupo Pumice Fall (Walker, 1980), Cotapaxi Layer 5 (Biass and Bonadonna, 2011; Biass et al., 2019), Hatepe tephra (Walker, 1981; Fierstein and Nathenson, 1992), Minoan tephra (Pyle, 1990; Daggitt et al., 2014), and tephra from the 1980 Mt. St. Helens eruption (Sarna-Wojcicki et al., 1981; Fierstein and Nathenson, 1992). They are chosen as their volumes and extents are different in magnitude, and the number of their isopachs varies from three to twelve. They represent tephras from island settings, where tephra measurements are typically limited where it falls in the sea (e.g., Taupo tephra) and where access to the volcanic island is limited (e.g., tephra from the 1815 Tambora eruption), and in continental settings, where a more complete distribution of isopachs are available (e.g., the 1980 Mt. St. Helens tephra). We consider them covering characteristics of most isopach datasets. More information about these datasets is given in Table 1, and the isopach data are presented in Tables 5 and 6.

2.3 Parameters

We apply the one-, two-, and (N-1)-segment exponential, power-law, and Weibull curves to the six isopach datasets. Parameters of the fitted curves are given in Table 2, and the fitted curves are shown in Fig. 3. Some of them are directly referenced from previous studies, and the others are updated in this work.

For the 1815 Tambora tephra which only has three isopachs, the parameters of its fitted curves are from Kandlbauer and Sparks (2014). Parameters of fitted curves for the Cotapaxi Layer 5 are from Biass and Bonadonna (2011) and Bonadonna and Costa (2012). Parameters of the one- and two-segment exponential curves for the rest of the datasets are from Fierstein and Nathenson (1992). The m and T_{pl} in the power-law curve (Eq. 3) are updated for the Hatepe dataset. The power-law curve does not fit well to the Taupo Pumice Fall, Minoan, and 1980 Mt. St. Helens tephra datasets, and is thus not adopted here. Parameters of the Weibull curves for the Taupo Pumice Fall, Hatepe, and Minoan deposits are updated to best fit the data using the Excel Spreadsheet provided in Bonadonna and Costa (2012). Parameters of the Weibull curve for the 1980 Mt. St. Helens tephra are referenced from Bonadonna and Costa (2012). We note here that a high standard is adopted to determine whether a curve fits the isopach data well: the curves need to fit the data visually well on the log(thickness) $-$ $\sqrt{\text{isopach area}}$ plot, and the predictions from the curves are characterized by high correlation coefficients with the isopach data (Table 4; all greater than 0.936 in non-logged thickness). This is necessary because we are interested in the presence of the two sources of uncertainty when the fitted curves seem to perform well.

2.4 Volume calculation and distribution with respect to $\sqrt{\text{isopach area}}$

We calculate the total volume (Table 3) and volume distribution with respect to $\sqrt{\text{isopach area}}$ based on the fitted curves using the trapezoidal rule (Fig. 2a). The fitted curves are discretized to 0.5 or 1 km-length $\sqrt{\text{isopach area}}$ segments, and the volume within each segment is calculated using Eq. 5. The maximum $\sqrt{\text{isopach area}}$ for each deposit in this calculation, i.e., the upper integration limit for the volume calculation, is given in Table 1, which is at least $\sim$4 times greater than the $\sqrt{\text{thinnest isopach area}}$ of the respective datasets.

Different integration limits are specified for the power-law and Weibull (only for the 1815 Tambora tephra as the corresponding Weibull curve leads to significantly great thickness) curves to be consistent with previous works and to avoid unrealistically large thickness values. Different proximal integration limits (e.g., 1, 2, 4 km $\sqrt{\text{isopach area}}$) are specified for the power-law curves of the 1815 Tambora tephra, Cotopaxi Layer 5, and Hatepe tephra datasets to account for its impact on the volume estimation. Proximal integration limits of the 1815 Tambora tephra are specified based on different thicknesses (thickness below 200, 150, and 120 cm), rather than by $\sqrt{\text{isopach area}}$, to be consistent with the work of Kandlbauer and Sparks (2014). The same proximal integration limit is applied to the fitted Weibull curve of this deposit. Distal integration limits for the power-law curves are specified from previous works as 300 km for the Cotapaxi Layer 5 (Biass and Bonadonna, 2011), 1000 km for the Hatepe tephra (Bonadonna and Houghton, 2005), and 1500 km for the 1815 Tambora tephra (Kandlbauer and Sparks, 2014).

All volume estimates from this work are consistent with previous estimates calculated from analytical integration (Table 2). The volume distributions with respect to $\sqrt{\text{isopach area}}$ based on the fitted curves are given in Fig. 4 for each deposit.

3 The model uncertainty

Misfit occurs because deviation between the isopach data and the fitted curves inevitably exists. This is due to uncertainty in both the isopach data and model. In the context of this work, where the former is temporarily assumed to be zero, the latter becomes more apparent (which does not mean that it is not significant otherwise): we cautiously construct isopachs such that they represent the true thicknesses and isopach areas of the deposit at the corresponding levels, but then we use the fitted curves that inevitably deviate or even fit poorly (see paragraph below) to the isopach data to estimate the tephra volume.

Practically, the curve fitting process is done based on log-transformed thickness and square root of isopach area. A curve that seems to fit well on the log(thickness) $-\sqrt{\text{isopach area}}$ plot does not necessarily fit well to the original isopach data (e.g., a predicted $\sqrt{\text{isopach area}}$ that is 120% of the original $\sqrt{\text{isopach area}}$ corresponds to 144% of the original isopach area). This could be further exaggerated by the maximum thickness (at most hundreds of meters) to extent (a few to even more than a million square kilometers) ratio of tephra fall deposits being extremely low. A thickness difference of 0.5 cm between the isopach data and the fitted curve may seem small, but the small difference might span an extensive area, which could greatly affect the volume estimation.

3.1 Problem demonstration

We examine the fitting between the fitted curves and the isopach data to demonstrate that the misfit as a result of model uncertainty occurs commonly and could affect the tephra volume estimation. The high correlation coefficients ($0.936- > 0.999$; Table 4) between the non-logged thickness predictions of the fitted curves and the original data seem to suggest that all fitted curves are consistent with the isopach data.

The original isopach data and predictions from the fitted curves are compared in Tables 5 and 6. Excluding the one-segment exponential curve applied to Cotapaxi Layer 5 (because it can be better described by the two-segment exponential curve), out of the 98 predictions from different curves and for different deposits, there are 35 thickness predictions that are outside the $90-110\%$ range with respect to non-logged thicknesses of the original datasets. Examined based on the isopach area, there are 44 predictions that are outside the $90-110\%$ range. Among these outlier predictions, there are *eight* thickness and *twenty* isopach area predictions that are outside the $80-120\%$ range with respect to the original datasets with the maximum deviation of 55% (20-cm isopach for the Mt. St. Helens tephra with the Weibull curve) and 142% (20-cm isopach for the Cotapaxi Layer 5 with the power-law curve) in terms of thickness, and 16% (20-cm isopach for the Mt. St. Helens tephra with the Weibull curve) and 167% (200-cm isopach for the Minoan tephra with the Weibull curve) in terms of isopach area. These results suggest that the deviation between the isopach data and predictions from the fitted curves occurs commonly even when the fitted curves seem to perform well (e.g., as indicated by the high correlation coefficients), and hence prove the common presence of misfitted curves. The above results also show that for the same datasets, more predictions with greater misfit can be detected when examined based on the isopach area, showing practically the importance of examining the goodness-of-fit based on area rather than thickness.

The tephra volume range defined by different fitted curves for each deposit is shown in Table 7. The ratio of maximum and minimum volume difference to the maximum volume is also given. The volume estimates that require integration limits (i.e., the power-law or Weibull curve for the Tambora tephra) are not included here because their values could greatly affect the volume estimate (Fig. 6), making the corresponding results non-comparable. Except for the Taupo Plinian deposit (0.6%), the ratios range from 10.5 to 20.7%. (The low ratio for the Taupo deposit will be discussed later in the text.) Here we focus on the the 1815 Tambora and 1980 Mt. St. Helens tephra datasets, as they are the end members with respect to the volume difference ratio (20.7 and 10.5%), and also because the one-segment exponential (for the Tambora tephra) and Weibull (for the Mt. St. Helens tephra) curves fit the deposits relatively poorly (correlation coefficients of 0.967 and 0.936, respectively). For the 1815 Tambora eruption dataset with just three isopachs, the one-segment exponential curve greatly underestimates the thickest isopach and greatly overestimates the second thickest one (curve predictions: 73.9% and 142.4% of the thicknesses, and 53.9% and 141.4% of the isopach areas respectively). As a result, the volume estimate based on the one-segment exponential curve, 103.4 km^3 (Table 2), should not be used to characterize the deposit volume.

The 1980 Mt. St. Helens dataset provides an interesting case in which, depending on the perspective, the impact of the model uncertainty could be considered negligible or noteworthy. The 1980 Mt. St. Helens tephra dataset has 12 isopachs. The thickness and area ranges of the 12 isopachs are 20 to 0.05 cm and 200 to 167,000 km^2, respectively. The two- and (N-1)-segment exponential curves are highly consistent with the isopach data (correlation coefficient greater than 0.999) and with each other, leading to volume estimates of 1.13 and 1.14 km^3 (Fig. 5). The volume estimate from the Weibull curve (correlation coefficient: 0.936) is 1.02 km^3. The volume difference of -0.11(=1.02-1.13) km^3 seems small, but closer examination in Fig. 5 shows that it occurs almost entirely due to the misfit between the isopach data and the fitted Weibull curve. Fig. 5c shows the volume per $\sqrt{\text{isopach area}}$ difference between the two- and (N-1)-segment exponential curves, and between the Weibull and (N-1)-segment exponential curves. The absolute volume difference of the former is a lot smaller than that of the latter. For the latter pair, the largest volume difference arises from the misfit in the $\sqrt{\text{isopach area}}$ ranges of $\sim 0-24$ and $\sim 60-220$ km, which encloses the 20- and 10-cm, and 3-, 2-, and 1-cm isopachs, respectively. The Weibull curve estimates thicknesses of 11.03 and 8.31 cm for the 20- and 10-cm isopachs, and 2.48, 1.77, and 0.86 cm for the 3-, 2-, and 1-cm isopachs, respectively (see Table 6 for the predicted isopach area data). The misfit in the two $\sqrt{\text{isopach area}}$ ranges contributes to -0.12 km^3 of volume difference between the Weibull and (N-1)-segment exponential curves (this is greater than the total volume difference of -0.11 km^3 because for some $\sqrt{\text{isopach area}}$, the Weibull curve thickness is greater; e.g, the red shading area in Fig. 5c). For the second range (i.e., $\sqrt{\text{isopach area}}$ from 60 to 220 km), the misfits, namely -0.52, -0.23, and -0.14 cm for the 3-, 2-, and 1-cm isopachs respectively, may seem small, but due to the low thickness to extent ratio, this difference spans a wide area, leading to a non-negligible volume difference of -0.072 km^3, about 6.4% of the total volume.

Viewing the problem from another perspective, we can also state that the fitting of the Weibull curve is not ideal, but a volume estimate of 1.02 km^3 from it, which is not greatly different from other estimates, shows the robustness of the isopach-based method. In addition, the magnitude of other sources of uncertainty are likely to be greater, and hence override the uncertainty from the misfit. However, if not carefully treated and acknowledged, the model uncertainty from the Weibull curve (in this particular case) might introduce bias or augment the uncertainty in the final volume estimate. For example, if we consider the uncertainty in constructing isopachs, and quantify the 1980 Mt. St. Helens tephra volume uncertainty including the Weibull curve estimate, the volume uncertainty would partially “propagate around (as we consider the uncertainty in constructing isopachs here)" the Weibull curve estimate that is already inaccurately underestimated, leading to overestimated volume uncertainty. Moreover, omitting the model uncertainty makes the tephra volume uncertainty non-comparable among different deposits, as the impact of the model uncertainty on the total volume uncertainty may vary by deposits (Fig. 1b as a sketch example).

In contrast to the two examples discussed above, the fitted Weibull curve for the Minoan tephra does not fit well to its isopach data, but its impact on the volume estimate is negligible. Its predictions for the 400-, 300-, and 200-cm isopachs are 84.8%, 90.7% and 119.8% of the respective isopach thicknesses and 62.3%, 75.6%, and 166.9% of the respective areas, but they are extremely small areawise relative to the other isopachs. For example, the 200-cm isopach has an area of 124 km^2 ($\sqrt{\text{isopach area}}$: ∼11.1 km), while the next thinner isopach, the 30-cm isopach, has an area of 21710 km^2 ($\sqrt{\text{isopach area}}$: ∼147.3 km). The misfit for the thicker isopachs thus has negligible impact on the total volume (Fig. 4e). This example is briefly presented here to show that the impact of the model uncertainty on tephra volume estimation also depends on properties of the specific isopach dataset (e.g., isopachs thicknesses and areas, their numbers and spacing).

3.2 Proposed measures to better quantify the model uncertainty

We propose to use isopach area, rather than correlation coefficient, thickness, or log-thickness, to examine the goodness-of-fit for the fitted curves, and all fitted isopach areas should be reported. Curves that do not fit well to the isopach data should not be used for volume calculation, and the criteria for using or not using a certain curve should be specified. We acknowledge the practical difficulty of determining what is "fitting well to the data", and refrain from drawing a hard line on it. However, one intuitive, reasonable, and bottom line criterion is provided here: if half or more of the predictions from a certain fitted curve are outside the ±40% range with respect to the corresponding isopach areas, the curve should not be used for the volume calculation. Essentially, we advocate for maximizing the clarity of how the fitted results are reported such that poorly fitted curves would not be used for the volume estimation, and that the most-informed interpretation on the volume estimates can be made.

For a set of fitted curves that pass the above or other stricter criterion, we should use the envelope or union of the thickness from these curves to define the volume range and variability, rather than using volumes calculated from individual curves. The (N-1)-segment exponential curve should also be included. The union thickness of the curves (Fig. 2d and e) is defined by the range between the maximum and minimum thicknesses among all well-fitted curves for each $\sqrt{\text{isopach area}}$ value. The bounds of the union thickness for all $\sqrt{\text{isopach area}}$ value are two curves which can be used to define the tephra volume range and variability. This can be realized with the help of Eq. 5 and discretizing the curves as done in this work.

The justification of this proposition is that if a fitted curve can be used to calculate the total tephra volume, any subset of the curve should be qualified to calculate the local tephra volume. In this way, the model uncertainty could be better captured and quantified independently from the uncertainty in constructing isopachs. Indeed, this proposition neglects the individual thinning pattern of different curves. Even though the segmented exponential, power-law, and Weibull curves are proposed with certain justifications, none of them are always better than the others. The complexity of plume dynamics and tephra dispersal and deposition suggests that each of these curves might be a good, but definitely not always perfect, approximation to the true thinning pattern, justifying the proposition.

The proposed measures do not consider other sources of uncertainty, and hence can be easily coupled with methods that quantify the other uncertainty sources in tephra volume estimation with the isopach-based method (e.g., Biasse et al., 2014; Daggitt et al., 2014; Biass et al., 2019) without interrupting the uncertainty propagation. A sketch example is shown in Fig. 1c in which the uncertainty from constructing isopachs and the model uncertainty are hierarchically captured following the proposed idea.

3.2.1 Application

We compare volume ranges of the six deposits defined by individual curves (the (N-1)-segment exponential curve included) and by the proposed measure in Table 7. Curves that require the specification of integration limit are excluded due to their significant impact on tephra volume (Fig. 6). The one-segment exponential curve for the Tambora tephra which has been shown to fit poorly to the isopach data is excluded. This only leaves the two-segment exponential curve for the dataset (which is also the (N-1)-segment exponential curve as it only has three isopachs), and the volume range for the deposit is thus not calculated. For the Mt. St. Helens tephra, we calculate the volume variability (max-min volume) including and excluding the Weibull curve which does not fit well to the isopach data to show the effect of including ill-fitting curves. The volume variability is smaller if the Weibull curve is excluded using the proposed measure (volume variability of 0.05 and 0.15 km^3, respectively, excluding and including the Weibull estimate), and it is even smaller than the volume variability calculated based on individual curves (0.12 km^3; Weibull curve included). This shows again that neglecting the model uncertainty might lead to overestimated tephra volume uncertainty. For the other four datasets, their volume variabilities defined based on the proposed measure are all greater and theoretically more robust than those calculated based on the individual curves.

4 Uncertainty from extrapolation

The uncertainty from extrapolation is well-recognized in time-series and spatial data analysis. Tephra volumes can be separated into volumes estimated based on interpolation and extrapolation. In this work, we separate the tephra volume into three portions, namely the portion that is within the thickest isopach, the portion that is within the thickest and thinnest isopachs, and the portion that is outside the thinnest isopach. Their volumes are denoted as V_{prox}, V_{int}, and V_{dist}, respectively (Fig. 2b). V_{int} is the interpolation volume, and the sum of the other two corresponds to the extrapolation volume. The definition of V_{prox}, V_{int}, and V_{dist} is different from how Klawonn et al. (2014a) defined the three regions of tephra volume (sketch shown in Fig. 2c), but this would not affect any conclusions in this work: V_{dist} defined here is equivalent to Region B in Klawonn et al. (2014a), and the difference between V_{prox} and Region C equals to the difference between Region A and V_{int}, which is a constant solely determined by the thickest isopach (shaded area in Fig. 2b and c).

The interpolated (i.e. within isopach) thickness and volume can be examined by leave-one-out validation. However, this cannot be done for those from extrapolation. As the uncertainties associated with interpolation versus extrapolation are non-comparable, Klawonn et al. (2014a,b) suggested that better estimation of the volume would come from strategies that realistically extrapolate deposit thickness and volume for the proximal and distal portions of the deposit, rather than focusing on the best fit to the thickness versus square-root area values.

4.1 Problem demonstration

As this question has been pointed out in Klawonn et al. (2014a), we briefly demonstrate it with the six datasets. V_{prox}, V_{int}, and V_{dist} of each deposit based on each fitted curve are plotted as histograms in Fig. 6. V_{prox} calculated based on different integration limits are also marked. It is well-known that the distal integration limits for the power-law are difficult to specify and justify, we simply specify them based on previous works as stated previously.

Fig. 6 shows that ratios of the interpolation and extrapolation volumes to the total volume vary by the isopach datasets. Similarly, variabilities of V_{prox}, V_{int}, and V_{dist} based on different fitted curves also vary greatly for each dataset. These corroborate arguments from Klawonn et al. (2014a,b), which suggest that the extrapolation volume and its uncertainty could have a big impact on the total volume estimation.

In addition, Fig. 6 shows that the variability of V_{prox} could be significantly affected by the proximal integration limit when it needs to be specified for a certain curve (i.e., the power-law or Weibull curve for the Tambora tephra in this study). This is shown in the 1815 Tambora, Cotapaxi Layer 5, and Hatepe tephra datasets (Fig. 6a, c, and d).

4.1.1 Underestimated uncertainty

Not properly addressing the extrapolation uncertainty could also lead to underestimated volume uncertainty. For a set of isopach data, two different fitted curves could provide similar estimates for the extrapolated thickness and volume, but this does not necessarily suggest that the uncertainty on the extrapolated volume is small. This can be illustrated with the Taupo tephra dataset. The fitted one-segment and Weibull curves both fit the isopach data well (Tables 5 and 6), and the predicted thinning patterns from the two curves are highly consistent with each other (Fig. 3b). Ranges of V_{prox}, V_{int}, and V_{dist} defined by the two curves are 0.36-0.52, 5.33-5.59, and 1.84-1.90 km^3, respectively. These seem to suggest that variabilities of V_{prox} and V_{dist} are small, and the extrapolated volume is subject to limited uncertainty. These statements are not accurate, because the one-segment and Weibull curves both fit well to the isopach data, but it is likely that they *happen* to be consistent with each other for the extrapolated thickness. The extrapolated thickness from the two is possibly not consistent with the true thinning pattern of the deposit. In such circumstances, the uncertainty of the extrapolated volume is underestimated or the volume estimate is subject to bias.

4.2 Proposed measures to better understand uncertainty from extrapolation

We concur the proposition by Klawonn et al. (2014a) that tephra volumes from interpolation and extrapolation should be reported separately. We recommend that measure to address model uncertainty proposed in this work should be applied to report ranges of V_{prox}, V_{int}, and V_{dist}.

We also propose that instead of trying to quantify the uncertainty for V_{prox} and V_{dist}, it is more objective and accurate to describe the uncertainty from extrapolation as uncertainty that cannot be better and robustly quantified based on the given isopach data. Hence, we can only test whether the total tephra volume is sensitive to the potential variability of V_{prox} and V_{dist}, i.e., treat it as a sensitivity test.

To implement the sensitivity test, we propose to first calculate the tephra volume changes by manually setting the maximum thickness (for V_{prox}) and extrapolated isopach area for a certain thickness (for V_{dist}) to different values, and calculate ratios of the volume changes to the total tephra volume. We denote the two volume differences as ΔV_{prox} and ΔV_{dist} and the two ratios as r_{prox} and r_{dist} (Fig. 2f). As r_{prox} and r_{dist} are ratios, their values are comparable among different isopach datasets. Larger r_{prox} and r_{dist} indicate that the total volume is more sensitive to the potential variability of V_{prox} and V_{dist}, respectively. We first define $T_{0,N-1}$ and $A_{0.5*\mathrm{Nth},N-1}$ as the maximum thickness and the isopach area of half of the thinnest isopach thickness inferred based on the (N-1)-segment exponential curve, respectively. ΔV_{prox} and ΔV_{dist} are defined as (Fig. 2f):

- ΔV_{prox}: the difference between the volumes calculated based on the $(N-1)$-segment exponential curve assuming $T_{0,N-1}$ to be (a) its original value calculated based on the (N-1)-segment exponential curve and (b) five times of its original value;
- ΔV_{dist}: the difference between the volumes calculated based on the $(N-1)$-segment exponential curve assuming $A_{0.5*\mathrm{Nth},N-1}$ to be (a) its original value calculated based on the (N-1)-segment exponential curve and (b) one and a half times of its original value.

r_{prox} and r_{dist} are defined as the ratios of ΔV_{prox} and ΔV_{dist} to the total tephra volume calculated based on the (N-1)-segment exponential curve. The denominator is chosen such that curve-fitting process can be avoided. In this way, the impact of misfit would not affect values of r_{prox} and r_{dist}. $T_{0,N-1}$ and $A_{0.5*\mathrm{Nth},N-1}$ are important for calculating r_{prox} and r_{dist}, but they are defined based on the (N-1)-segment exponential curve. That is to say, their values only depend on the two thickest and two thinnest isopachs. This is again a compromise we have to take to avoid curve-fitting. We have tried defining ΔV_{dist} based on manually changing the isopach area of the 0.01-cm isopach, and the resultant values of r_{dist} are similar compared to the current way of defining ΔV_{dist}.

It is possible that the true maximum thickness and isopach area of half of the thinnest isopach thickness exceed what are assumed in defining ΔV_{prox} and ΔV_{dist}. This is likely to occur especially when the deposit can be characterized by a two-segment exponential curve, and the existing isopachs only cover the proximal or distal portion of the deposit. If that happens, it can be recognized by experienced users. Moreover, in such cases, values of r_{prox} and r_{dist} could still be alarmingly large because their values depend not only on the assumed thickness and isopach area ranges, but also on the total tephra volume (calculated based on the given isopachs), thicknesses and areas of the thickest and thinnest given isopachs. This will be demonstrated below.

As noted earlier, large r_{prox} and r_{dist} indicate that the total volume is sensitive to the potential variability of V_{prox} and V_{dist}. Based on our analysis with the six datasets given below, we are confident that the total volume is greatly sensitive to V_{prox} or V_{dist} if its value is above 0.4. This does not suggest that the volume is insensitive if otherwise.

4.2.1 Application

We calculate r_{prox} and r_{dist} for the six tephra datasets plus the Minoan and 1980 Mt. St. Helens tephra datasets with selected isopachs (Table 8). The latter two tephra datasets can be well-characterized by two-segment exponential curves. In addition to r_{prox} and r_{dist} based on all of their isopachs, we calculate r_{prox} and r_{dist} based on their isopachs that only display the proximal (four thickest isopachs for both) and distal (four and six thinnest isopachs for the two datasets, respectively) thinning patterns to check how r_{prox} and r_{dist} respond to such circumstances. This is necessary because, as mentioned earlier, the *true* maximum thickness and *true* isopach area of half of the thinnest isopach thickness might exceed the ranges assumed in defining r_{prox} and r_{dist} given only the proximal or distal isopachs.

For the datasets with the complete isopachs, we highlight datasets with the greatest r_{prox} and r_{dist}. The 1815 Tambora tephra and the Cotopaxi Layer 5 lead to the greatest r_{prox} (0.681 and 0.693). They have large r_{prox} because: the 1815 Tambora tephra dataset has its thickest isopach (20 cm) with a relatively large area of 144,964 km^2. The uncertainty of its thinning pattern within the thickest isopach could significantly affect the total volume; For Cotopaxi Layer 5, its thickest (100 cm) and second thickest (50 cm) isopachs imply that the deposit may have a very rapid thinning rate within the thickest isopach (Fig. 3c). Its V_{int} is relatively small, and the true V_{prox} value could take up a large portion of the total volume (Fig. 6c). Its potential variability thus would greatly affect the total deposit volume. The Tambora and Cotapaxi Layer 5 tephra datasets have similarly large r_{prox} values, suggesting that the sensitivity of their total volumes to their V_{prox} is great and at the same level. The two deposits are different in volume, thinning pattern, and number of isopachs, but the proposed measure enables directly comparing the total volume sensitivity to V_{prox}.

The Taupo Plinian deposit is characterized by the greatest r_{dist} (0.437). Its thinnest isopach corresponds to a thickness of 12.5 cm. How the deposit thins beyond this isopach and the potential variability of V_{dist} are uncertain and could greatly impact the total volume estimate. The high value of r_{dist} for the Taupo deposit suggests that the total volume is sensitive to V_{dist}. As mentioned earlier, this cannot be reflected if we simply examine V_{dist} estimated based on the fitted curves that possibly happen to be consistent with each other, showing the effectiveness of the proposed measure.

The Minoan and 1815 Tambora tephra datasets have the lowest r_{prox} (0.001) and r_{dist} (0.041), respectively. For the former, its thickest isopach is small area-wise (600 cm, 9 km^2), and the thinnest isopach (5 cm) has an area of 191,710 km^2. A significant portion of its volume is from V_{int} and V_{dist}. Regardless of the thickness distribution within the thickest isopach, the total volume of the deposit would not be greatly affected by it and thus not sensitive to V_{prox}. For the 1815 Tambora tephra dataset, the thinnest isopach is thin and large areawise (0.1 cm, 4,288,784 km^2), which means that its V_{dist} has to be very small relative to the total volume, and hence would not greatly affect the total volume estimate.

Similarly, the 1980 Mt. St. Helens tephra dataset has 12 isopachs. Its thickest (20 cm) and thinnest (0.05 cm) isopachs have areas of 200 and 16,700 km^2, respectively. A large portion of the tephra volume belongs to V_{int}, leading to relatively low r_{prox} (0.065) and r_{dist} (0.101) for the deposit. Values of r_{prox} and r_{dist} for other deposits that are not mentioned above range from 0.1-0.4.

Given just proximal isopachs, how the distal Minoan and 1980 Mt. St. Helens tephras thin is unknown to us. Their proximal isopachs suggest a great thinning rate, which means that in such circumstances, the assumed isopach area range for calculating r_{dist} might be too small compared to the true values. r_{dist} for the two increase from 0.389 and 0.101 with the complete datasets to 0.609 and 0.575 given only the proximal isopachs, respectively. The latter two values are alarmingly large, indicating that the assumed volume variability for V_{dist} could take up more than half of the total volume given just the proximal isopachs. The total volume is sensitive to the potential variability of V_{dist} in this situation. r_{dist} could be alarmingly large here because r_{dist} depends on the total volume and ΔV_{dist}, which is a function of the thinnest isopach thickness and area in addition to the assumed isopach area range. Similarly, r_{prox} of the Minoan and 1980 Mt. St. Helens tephras increase greatly from 0.001 and 0.065 with the complete datasets to 0.238 and 0.442 given only the distal isopachs, respectively. This indicates that the total volume would be a lot more sensitive to the potential variability of V_{prox} if the proximal isopachs are unavailable, suggesting the effectiveness and robustness of the proposed measure in such circumstances. The above results indicate that values of r_{prox} and r_{dist} could effectively indicate whether the total volume is sensitive to the potential variability of V_{prox} and V_{dist} given isopach datasets of various coverage and quality.

5 Conclusions

In this work, we study two sources of uncertainty in estimating tephra volumes using the isopach-based method. The two occur because fitting certain curves to the isopach data on the log(thickness)$-\sqrt{\text{isopach area}}$ plot is needed for the method. The first source of uncertainty is the model uncertainty. It occurs because (1) there is no curve that could always fit perfectly well to the isopach data whether the data uncertainty exists or not and (2) the fitting is done based on log-transformed thickness and square root of isopach area, and as a result, curves that fit poorly to the isopach data could be used for the volume estimation without being noticed. If omitted, this source of uncertainty could introduce additional bias, or lead to under- or overestimated uncertainty for the volume estimate. The second source of uncertainty is from extrapolation, as originally proposed in Klawonn et al. (2014a). It occurs because the predicted thickness for each fitted curve is partially from interpolation and partially from extrapolation. The total tephra volume is the sum of volumes from extrapolation and interpolation, but the two are not comparable because the extrapolated thickness or volume cannot be validated based on data.

The two sources of uncertainty may not always greatly affect the volume estimate, especially in well-constrained datasets, but their importance can be proved theoretically. Different sources of uncertainty propagate hierarchically in tephra volume estimation. The two sources of uncertainty occur in the last step, i.e., during the curve-fitting process, before the volume calculation (i.e., volume integration). If they are omitted, the sources of uncertainty in previous steps of the hierarchy might not be properly inherited, potentially leaving the estimated uncertainty subject to misrepresentation (Fig. 1).

We use six tephra isopach datasets to demonstrate the presence of the two sources of uncertainty and show their impact on tephra volume estimation. Propositions to address them are given. For the model uncertainty, the goodness-of-fit should be evaluated based on isopach areas, and curves that do not fit well to the isopach data should not be used to characterize the tephra volume. We recommend a bottom line criterion that if half or more of the predictions from a fitted curve are outside the $\pm 40\%$ range with respect to the corresponding isopach areas, the curve should not be used for the volume estimation. For a set of curves that satisfy the above or stricter criterion, we propose to use the envelope (i.e., union) of the curves to define the volume range, instead of using volumes estimated from individual curves. Thus the model uncertainty is more accurately captured. This proposed measure can be easily incorporated into methods that quantify other sources of uncertainty in estimating tephra volumes with the isopach-based method. For the uncertainty from extrapolation, we concur to Klawonn et al. (2014a) that volumes from interpolation and extrapolation should be reported separately. We propose that the uncertainty from extrapolation should be addressed as a sensitivity test. We calculate tephra volume changes by assuming different maximum thicknesses and different isopach areas for half of the thinnest isopach thickness, and use the ratios (r_{prox} and r_{dist}) of the two volume differences to the total tephra volume to show if and how the total volume is sensitive to the extrapolated volumes within the thickest and outside the thinnest isopachs, respectively. We propose that r_{prox} or r_{dist} being greater than 0.4 indicates strong sensitivity of total volume to the volume within the thickest (V_{prox}) or outside the thinnest (V_{dist}) isopachs. Proposed measures to address the two sources of uncertainty are tested against the six isopach datasets, and are proved to be effective. We hope that this work could help quantify tephra volume uncertainty in a more robust and accurate way, and make tephra volume uncertainty comparable across different tephra deposits in future works when the isopach-based method is used.

6 Tables

Table 1: Information for isopach data used in this work. References for the isopachs and isopach data (i.e., isopach area and thickness) are reported separately.

Tephra deposit/ eruption (# of isopachs)	Isopach area$^{1/2}$ range modeled (km)	Thinnest isopach area$^{1/2}$ (km)	Exponential, power law, and Weibull volume estimates from previous works(km^3)	Features	Isopachs constructed in	Isopach area reference
1815 Tambora eruption (3)	1-8000	2070	103, 90, 602 [1]	Isopach thickness range: 20-0.1 cm Sparse isopachs; No proximal isopachs.	Kandlbauer and Sparks, 2014.	Kandlbauer and Sparks, 2014.
Taupo Pumice Fall (5)	1-5000	123	6.7, 26, 12 [2]	Isopach thickness range: 150-12.5 cm; No distal isopachs.	Walker, 1980.	From digitization; Consistent with data plotted in Pyle (1989).
Cotapaxi Layer 5 (6)	0.5-1000	25	0.3, 0.45, 0.23 [2]	Isopach thickness range: 100-5 cm.	Biass and Bonadonna, 2011.	Biass and Bonadonna, 2011; Biass et al, 2019.
Hatepe (7)	0.5-2000	96	1, 1.5, 0.56 [2]	Isopach thickness range: 200-3 cm.	Walker, 1981.	Fierstein and Nathenson, 1992.
Minoan (8)	1-3000	437	44, 87, 42 [2]	Isopach thickness range: 600-5 cm; Four very proximal isopachs plus four distal isopachs.	Pyle 1990.	Matthew Daggitt; David Pyle; Tamsin Alice Mather (2014), "AshCalc," https://vhub.org/resources/ashcalc.
1980 Mt. St. Helens (12)	1-2000	408	1.1, 1.2, 1.0 [2]	Isopach thickness range: 20-0.05 cm; Display distinct two-segments features.	Sarna-Wojcicki et al, 1981.	Fierstein and Nathenson, 1992.

[1] Kandlbauer and Sparks, 2014; [2] All data from Table 1 of Bonadonna and Costa, 2012. Volume estimates from exponential and power-law curves have slight deviations compared to data listed in Fierstein and Nathenson (1992) and Bonadonna and Houghton (2005). We select data in Table 1 of Bonadonna and Costa (2012) for consistency, and they would not affect any conclusions in this work.

Table 2: Parameters for curves used in this work.

Dataset (no. of isopachs)	One-segment exponential		Two-segments exponential			Power-law		Weibull			References
	T_0 (cm)	k (km^{-1})	T_0; T_1 (cm)	$A^{1/2}_{ip}$ (km)	k; k_1 (km^{-1})	T_{pl} (cm)	m	θ (cm)	λ (km)	n	
1815 Tambora eruption (3)	46	0.0030	-	-	-	$29695*10^5$	3.154	5000	51.34	0.438	Kandlbauer and Sparks, 2014.
Taupo Plinian deposit (5)	197	0.0225	-	-	-	-	-	59.06 [2]	96.85 [2]	1.43 [2]	Fierstein and Nathenson (1992); Bonadonna and Houghton (2005).
Cotopaxi L5 (6)	224	0.1500	1383; 171	9	0.37; 0.14	5936	2.11	74.9	13.6	1.2	Biass and Bonadonna (2011); Bonadonna and Costa (2012).
Hatepe (7)	-	-	480; 35	61	0.069; 0.0256	81389 [1]	2.20 [1]	139.04 [2]	29.82 [2]	0.82 [2]	Fierstein and Nathenson (1992); Bonadonna and Costa (2012).
Minoan (8)	-	-	890; 73	21	0.127; 0.0062	-	-	22.42 [2]	350.68 [2]	1.31 [2]	Fierstein and Nathenson (1992); Bonadonna and Costa (2012).
1980 Mt. St. Helens (12)	-	-	76; 8.4	27	0.094; 0.0126	-	-	2.44	169.9	1.38	Fierstein and Nathenson (1992); Bonadonna and Costa (2012).

[1] linear regression based on the log-scaled thickness and square root of isopach area; [2] estaimted using Excel spreadsheet from Bonadonna and Costa (2012).

Table 3: Tephra volumes calculated based on curves used in this work. For the power-law curve, different proximal integration limits are used to test whether they are sensitive to the total volume. The Weibull curve for the Tambora tephra also adopts a proximal integration limit to avoid unrealistically large thickness and volume prediction.

Dataset (no. of isopachs)	Estimated volume based on different fitted curves (km^3)				
	One-segment exponential	Two-segments exponential	Power-law	Weibull	(N-1)-segment exponential
1815 Tambora eruption (3)	103.4	130.4	Thickness< 120 cm & 0.5 km < Isopach area$^{0.5}$ <1500 km: 90.8 [1] Thickness< 150 cm & 0.5 km < Isopach area$^{0.5}$ <1500 km: 99.5 Thickness< 200 cm & 0.5 km < Isopach area$^{0.5}$ <1500 km: 111.8	Total: : > 500 [1] Thickness < 120 cm: 105.5 Thickness < 150 cm: 113.0 Thickness < 200 cm: 123.8	130.4
Taupo Plinian deposit (5)	7.8 [2]	-	-	7.7 [3]	7.8
Cotopaxi L5 (6)	-	0.28	0 km < Isopach area$^{0.5}$ < 300 km: 0.71 1 km < Isopach area$^{0.5}$ < 300 km: 0.51 4 km < Isopach area$^{0.5}$ < 300 km: 0.42 16 km < Isopach area$^{0.5}$ < 300 km: 0.35	0.23	0.28
Hatepe (7)	-	2.5 [2]	0 km < Isopach area$^{0.5}$ < 1000 km: 9.1 1 km < Isopach area$^{0.5}$ < 1000 km: 6.1 2 km < Isopach area$^{0.5}$ < 1000 km: 5.0 4 km < Isopach area$^{0.5}$ < 1000 km: 4.1	3.0 [3]	2.5
Minoan (8)	-	38.5 [2]	-	42.1	45.5
1980 Mt. St. Helens (12)	-	1.1	-	1.0	1.1

[1] Integration limits to be consistent with Kandlbauer and Sparks, 2014
[2] Different from values listed in Bonadonna and Costa, 2012, but consistent with Fierstein and Nathenson, 1992
[3] Different from value estimated in Bonadonna and Costa, 2012, but based on a better fitted curve

Table 4: Correlation coefficients between the non-logged isopach thickness and thickness predicted by different fitted curves.

Dataset (no. of isopachs)	One-segment exponential	Two-segments exponential	Power-law	Weibull
1815 Tambora eruption (3)	0.967	-	>0.999	>0.999
Taupo Plinian deposit (5)	0.996	-	-	0.995
Cotopaxi L5 (6)	0.961	0.999	0.991	0.973
Hatepe (7)	-	>0.999	0.974	0.991
Minoan (8)	-	0.998	-	0.992
1980 Mt. St. Helens (12)	-	>0.999	-	0.936

Table 5: Original isopach data and thicknesses predicted by different fitted curves for the tephra datasets. Ratios of prediction to original data are also given. Predictions that are $80-90\%$ or $110-120\%$ with respect to the original data are marked in blue, and the ones that are below 80% or above 120% with respect to the isopach data are marked in red.

Dataset	Thickness (cm)	Hand-drawn Isopach area (km^2)	One-segment exponential		Two-segment exponential		Power-law		Weibull	
			Predicted thickness (cm)	Prediction/ hand-drawn isopach thickness	Predicted thickness (cm)	Prediction/ hand-drawn isopach thickness	Predicted thickness (cm)	Prediction/ hand-drawn isopach thickness	Predicted thickness (cm)	Prediction/ hand-drawn isopach thickness
Tambora	20	144964	14.78	73.9%			21.55	107.7%	19.73	98.7%
	5	391219	7.12	142.4%			4.50	90.0%	5.07	101.4%
	0.1	4288784	0.10	95.0%			0.10	103.2%	0.10	99.5%
Taupo	150	242	138.82	92.5%					155.67	103.8%
	100	1012	96.30	96.3%					90.89	90.9%
	50	2922	58.38	116.8%					53.34	106.7%
	25	8229	25.59	102.4%					24.66	98.6%
	12.5	15256	12.23	97.9%					12.48	99.8%
Cotapaxi Layer 5	100	49	78.39	78.4%	103.75	103.8%	97.80	97.8%	81.19	81.2%
	50	79	58.95	117.9%	51.37	102.7%	58.92	117.8%	57.64	115.3%
	30	151	35.40	118.0%	30.56	101.9%	29.77	99.2%	33.45	111.5%
	20	303	16.47	82.4%	14.96	74.8%	14.32	71.6%	16.04	80.2%
	10	458	9.04	90.4%	8.55	85.5%	9.25	92.5%	9.31	93.1%
	5	650	4.89	97.7%	4.81	96.3%	6.39	127.9%	5.40	108.1%
Hatepe	200	170			196.24	98.1%	284.27	142.1%	222.18	111.1%
	100	530			98.94	98.9%	81.24	81.2%	84.04	84.0%
	50	1100			49.33	98.7%	36.35	72.7%	41.19	82.4%
	25	1780			26.56	106.3%	21.39	85.6%	24.44	97.8%
	12	2970			11.42	95.2%	12.17	101.4%	13.25	110.4%
	6	4800			5.94	99.0%	7.17	119.5%	6.99	116.4%
	3	9300			2.96	98.8%	3.46	115.4%	2.54	84.6%
Minoan	600	9			604.21	100.7%			591.06	98.5%
	400	46			376.10	94.0%			339.24	84.8%
	300	86			273.16	91.1%			272.03	90.7%
	200	124			216.37	108.2%			239.70	119.8%
	30	21710			29.28	97.6%			29.58	98.6%
	20	44073			19.86	99.3%			19.17	95.9%
	10	99370			10.34	103.4%			10.11	101.1%
	5	191710			4.83	96.7%			5.05	101.0%
Mt. St. Helens	20	200			20.11	100.6%			11.03	55.2%
	10	460			10.12	101.2%			8.31	83.1%
	7	640			7.05	100.7%			7.39	105.6%
	6	840			5.83	97.2%			6.69	111.6%
	4	2500			4.47	111.8%			4.33	108.2%
	3	7600			2.80	93.3%			2.48	82.6%
	2	12800			2.02	101.0%			1.77	88.7%
	1	30000			0.95	94.7%			0.86	86.3%
	0.5	48000			0.53	106.3%			0.50	100.7%
	0.25	79000			0.24	97.3%			0.24	96.4%
	0.1	118000			0.11	110.8%			0.11	112.3%
	0.05	167000			0.05	97.5%			0.05	98.6%

Table 6: Original isoapch data and isopach areas predicted by different fitted curves for the tephra datasets. Ratios of prediction to original data are also given. Predictions that are $80-90\%$ or $110-120\%$ with respect to the original data are marked in blue, and the ones that are below 80% or above 120% with respect to the isopach data are marked in red.

Dataset	Thickness (cm)	Hand-drawn Isopach area (km^2)	One-segment exponential		Two-segment exponential		Power-law		Weibull	
			Predicted isopach area (km^2)	Prediction/ hand-drawn isopach area	Predicted isopach area (km^2)	Prediction/ hand-drawn isopach area	Predicted isopach area (km^2)	Prediction/ hand-drawn isopach area	Predicted isopach area (km^2)	Prediction/ hand-drawn isopach area
Tambora	20	144964	78160	53.9%			151975	104.8%	143493	99.0%
	5	391219	553237	141.4%			366055	93.6%	394901	100.9%
	0.1	4288784	4218168	98.4%			4374112	102.0%	4276296	99.7%
Taupo	150	242	147	60.6%					270	111.6%
	100	1012	908	89.7%					806	79.6%
	50	2922	3714	127.1%					3250	111.2%
	25	8229	8418	102.3%					8109	98.5%
	12.5	15256	15020	98.5%					15236	99.9%
Cotapaxi Layer 5	100	49	29	59.0%	50	102.9%	48	97.9%	35	72.4%
	50	79	100	126.2%	81	101.6%	93	116.8%	95	120.0%
	30	151	180	118.7%	155	102.2%	150	99.3%	170	112.1%
	20	303	259	85.7%	235	77.6%	221	72.9%	251	82.8%
	10	458	430	93.8%	411	89.8%	426	92.9%	435	95.1%
	5	650	643	98.8%	637	97.9%	821	126.2%	681	104.7%
Hatepe	200	170			163	95.8%	234	137.6%	194	114.0%
	100	530			523	98.7%	439	82.8%	438	82.6%
	50	1100			1087	98.8%	823	74.9%	910	82.7%
	25	1780			1855	104.2%	1545	86.8%	1745	98.0%
	12	2970			2892	97.4%	3008	101.3%	3210	108.1%
	6	4800			4746	98.9%	5644	117.6%	5339	111.2%
	3	9300			9210	99.0%	10590	113.9%	8401	90.3%
Minoan	600	9			10	103.6%			9	96.0%
	400	46			40	86.2%			29	62.3%
	300	86			73	84.8%			65	75.6%
	200	124			138	111.4%			207	166.9%
	30	21710			20572	94.8%			21165	97.5%
	20	44073			43609	98.9%			41382	93.9%
	10	99370			102800	103.5%			100593	101.2%
	5	191710			186990	97.5%			193255	100.8%
Mt. St. Helens	20	200			202	100.9%			32	15.8%
	10	460			466	101.2%			268	58.3%
	7	640			644	100.6%			744	116.3%
	6	840			730	86.9%			1124	133.8%
	4	2500			3467	138.7%			2986	119.4%
	3	7600			6677	87.9%			5384	70.8%
	2	12800			12972	101.3%			10737	83.9%
	1	30000			28530	95.1%			25837	86.1%
	0.5	48000			50140	104.5%			48267	100.6%
	0.25	79000			77802	98.5%			77285	97.8%
	0.1	118000			123659	104.8%			124491	105.5%
	0.05	167000			165375	99.0%			166120	99.5%

Table 7: Volume ranges of the six tephra deposits defined by individual fitted curves and by the proposed measure to address the model uncertainty (presented as max-min = variability). For the former, the volume variability divided by the maximum volume is given for reference. Volumes whose calculation requires the specification of integration limit are not included here to avoid additional complexity. For the 1980 Mt. St. Helens tephra dataset, crossed-out calculation is done including the Weibull curve. See text for more details.

Dataset	Vmax-Vmin = volume difference (km3)		
	Calculated based on individual curves	Volume difference/ Vmax (%)	Calculated based on proposed measure
1815 Tambora eruption	130.35-103.37=26.98	20.7%	-
Taupo Plinian deposit	7.80-7.75=0.05	0.6%	8.21-7.42=0.79
Cotopaxi L5	0.28-0.23=0.05	17.9%	0.30-0.21=0.09
Hatepe	2.97-2.45=0.52	17.5%	3.23-2.22=1.01
Minoan	45.50-38.51=6.99	15.4%	45.97-38.04=7.93
1980 Mt. St. Helens	1.14-1.02=0.12	10.5%	~~1.16-1.01=0.15~~ 1.16-1.11=0.05

Table 8: r_{prox} and r_{dist} of different isopach datasets. For the Minoan and 1980 Mt. St. Helens tephra datasets, the numbers in the brackets indicate the isopach subsets used for the calculation. For example, "Minoan (1-4)" means the four thickest isopachs of the Minoan dataset are used for calculation.

Dataset	Description	r_{prox}	r_{dist}
1815 Tambora eruption	All isopachs	0.681	0.041
Taupo Plinian deposit	All isopachs	0.049	0.437
Cotopaxi Layer 5	All isopachs	0.693	0.161
Hatepe	All isopachs	0.193	0.207
Minoan	All isopachs	0.001	0.389
1980 Mt. St. Helens	All isopachs	0.065	0.101
Minoan (1-4)	Proximal isopachs only	0.075	0.609
Minoan (4-8)	Distal isopachs only	0.238	0.444
1980 Mt. St. Helens (1-4)	Proximal isopachs only	0.260	0.575
1980 Mt. St. Helens (7-12)	Distal isopachs only	0.442	0.111

521 # 7 Figures

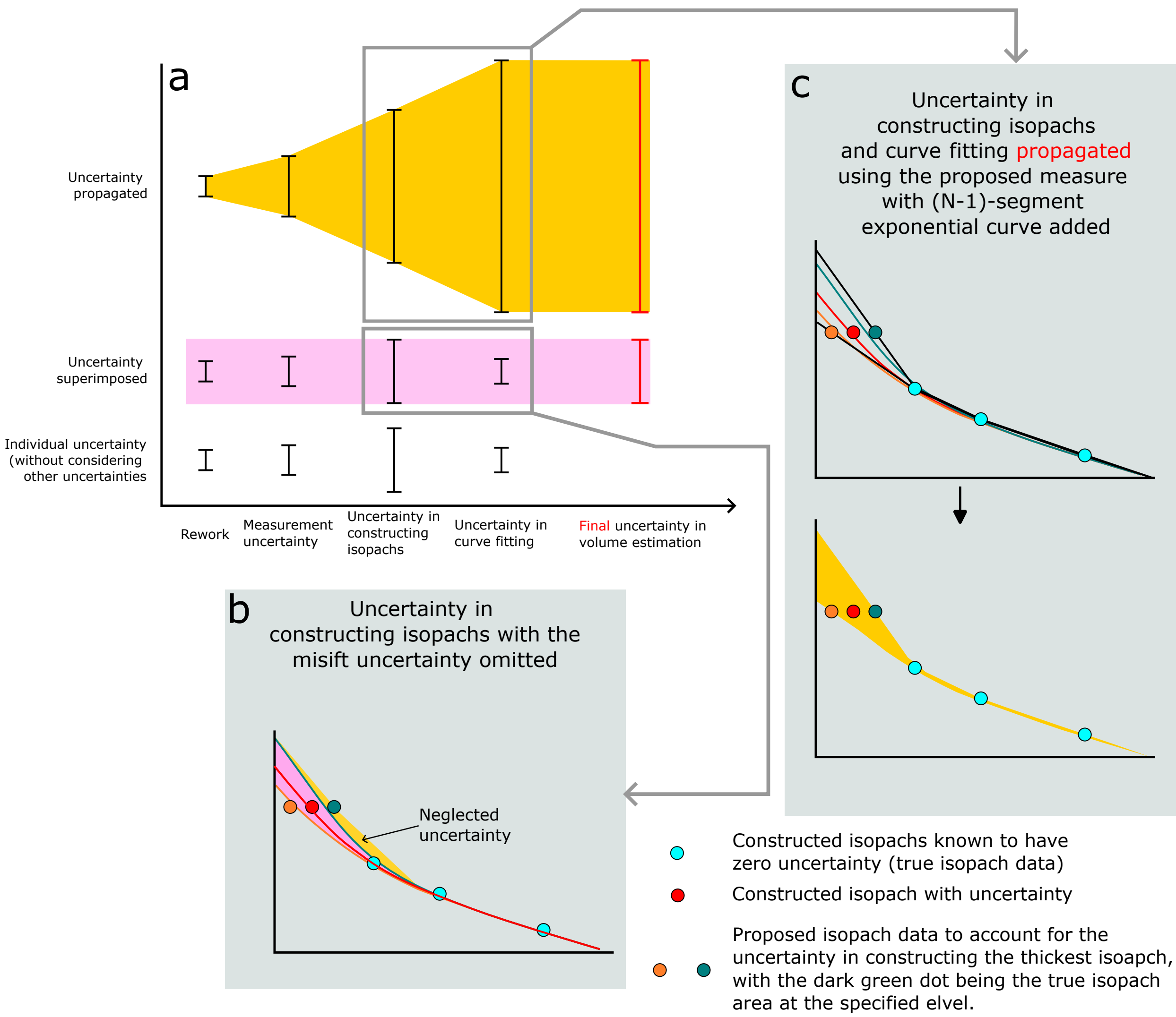

Figure 1: a: sketch showing the difference between different sources of uncertainty (x-axis) superimposed (pink polygon) and propagated following a hierarchical order (yellow polygon). The final volume uncertainty as a result of all these uncertainties superimposed or propagated is denoted as red bar. The black bars correspond to the uncertainty at each step of the hierarchy; Focusing just on the uncertainty from constructing isopachs and from model uncertainty, b shows the situation in which the model uncertainty is omitted: by varying the area of the thickest isopach, the estimated volume range defined by the three corresponding fitted curves does not cover the true tephra volume, as all three curves underestimate the thickest isopach area and thickness. In c, the two sources of uncertainty are propagated following the proposed idea. No additional curves that fit well to the data are plotted for simplicity. Two added (N-1)-segment exponential curves together with the three fitted curves define the yellow envelope which corresponds to the properly propagated volume uncertainty from the two sources of uncertainty.

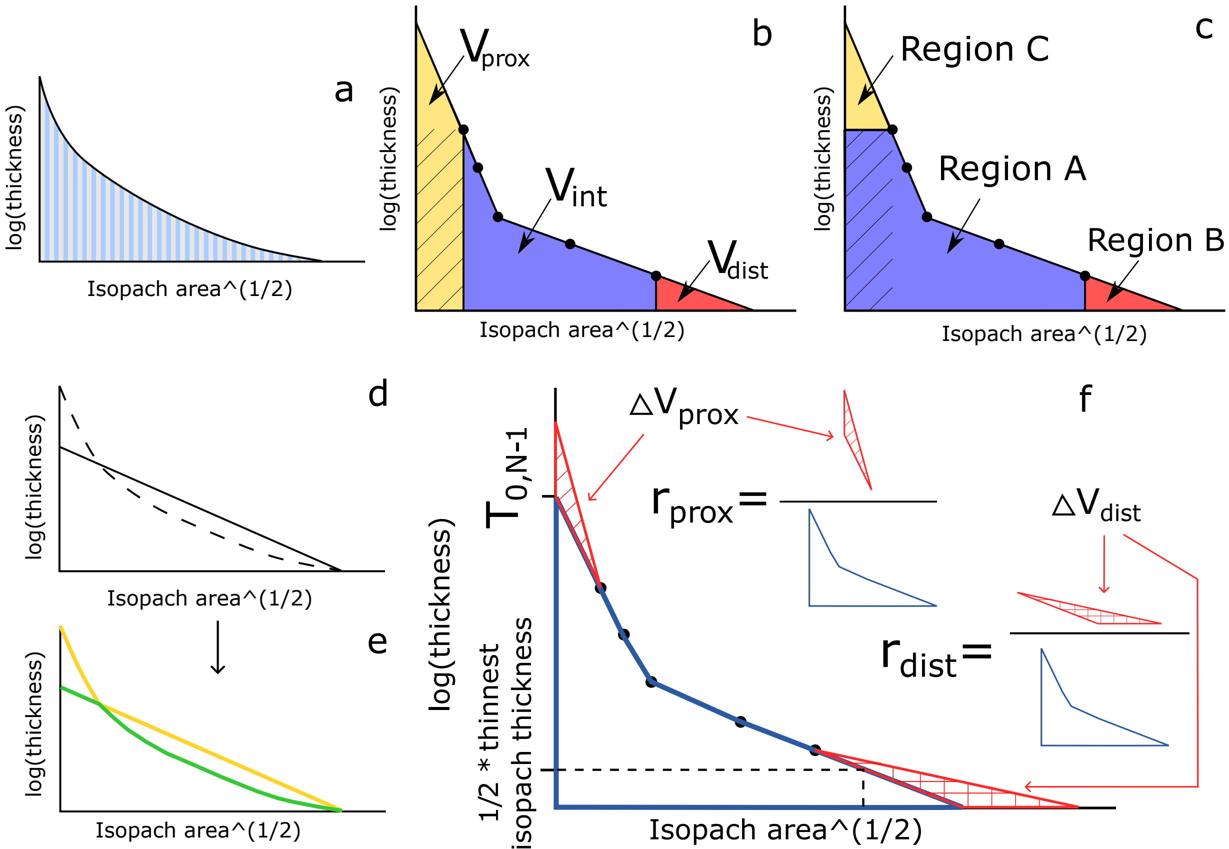

Figure 2: a: tephra volume is discretized as "vertical bars" and calculated with Eq. 5 using the trapezoidal rule; b: how V_{prox}, V_{int}, and V_{dist} are defined; c: how Regions A, B, and C are defined in Klawonn et al. (2014a). The shaded area is the difference between V_{prox} and Region C and also the difference between V_{int} and Region A; d and e: with two fitted curves that both fit well (based on a specified criterion) to the isopach data, instead of using the volumes from the two individual curves (as volumes of the solid and dashed lines in d), we propose to use the union or the envelop thickness defined by the two curves to constrain the volume from the curves (as volumes of the green and yellow lines in e); f: sketch showing how ΔV_{prox}, ΔV_{dist}, r_{prox}, and r_{dist} are defined.

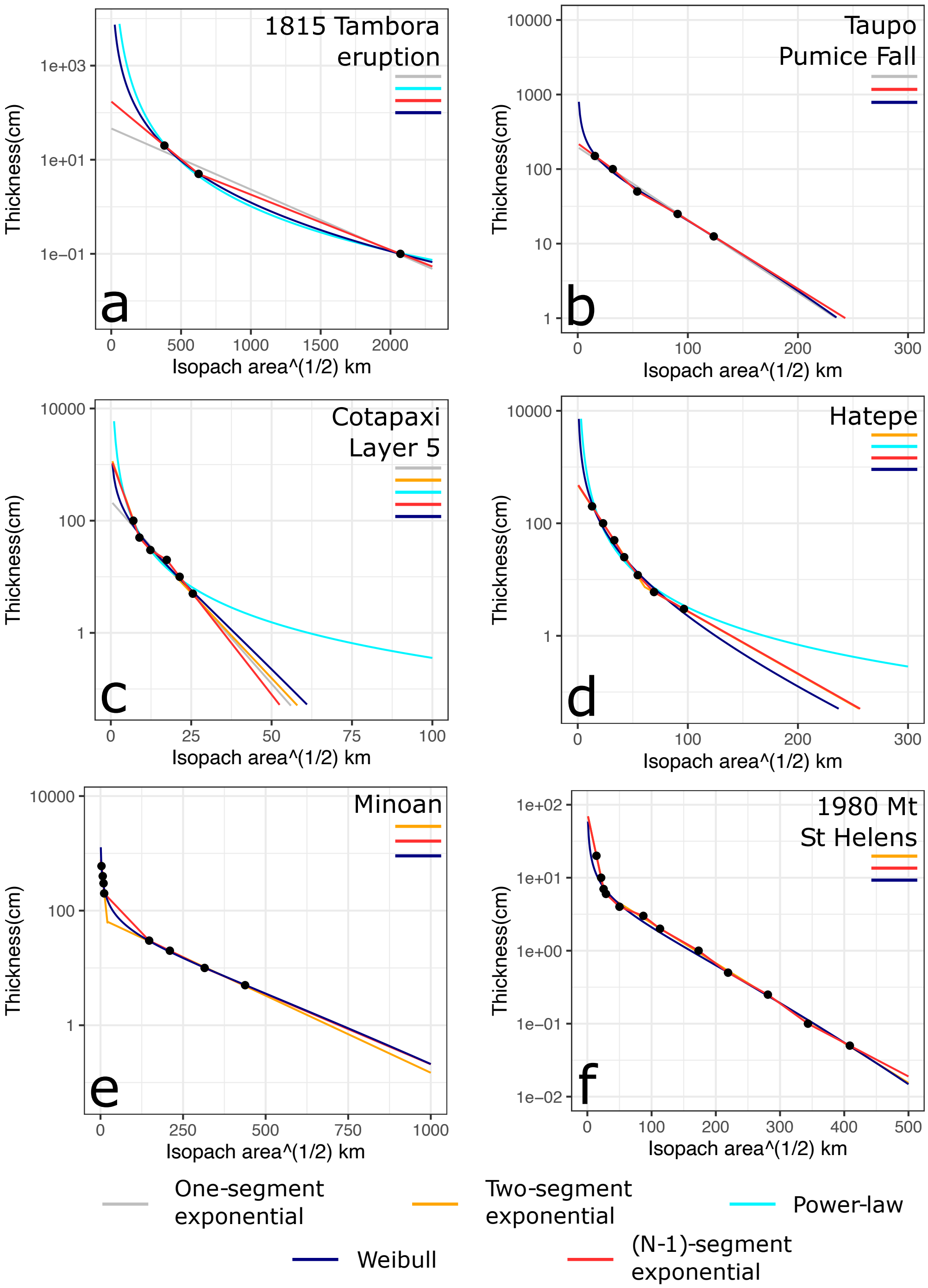

Figure 3: The log(thickness) $-$ $\sqrt{\text{isopach area}}$ plot showing the original isopach data and the fitted curves with their parameters given in Table 2.

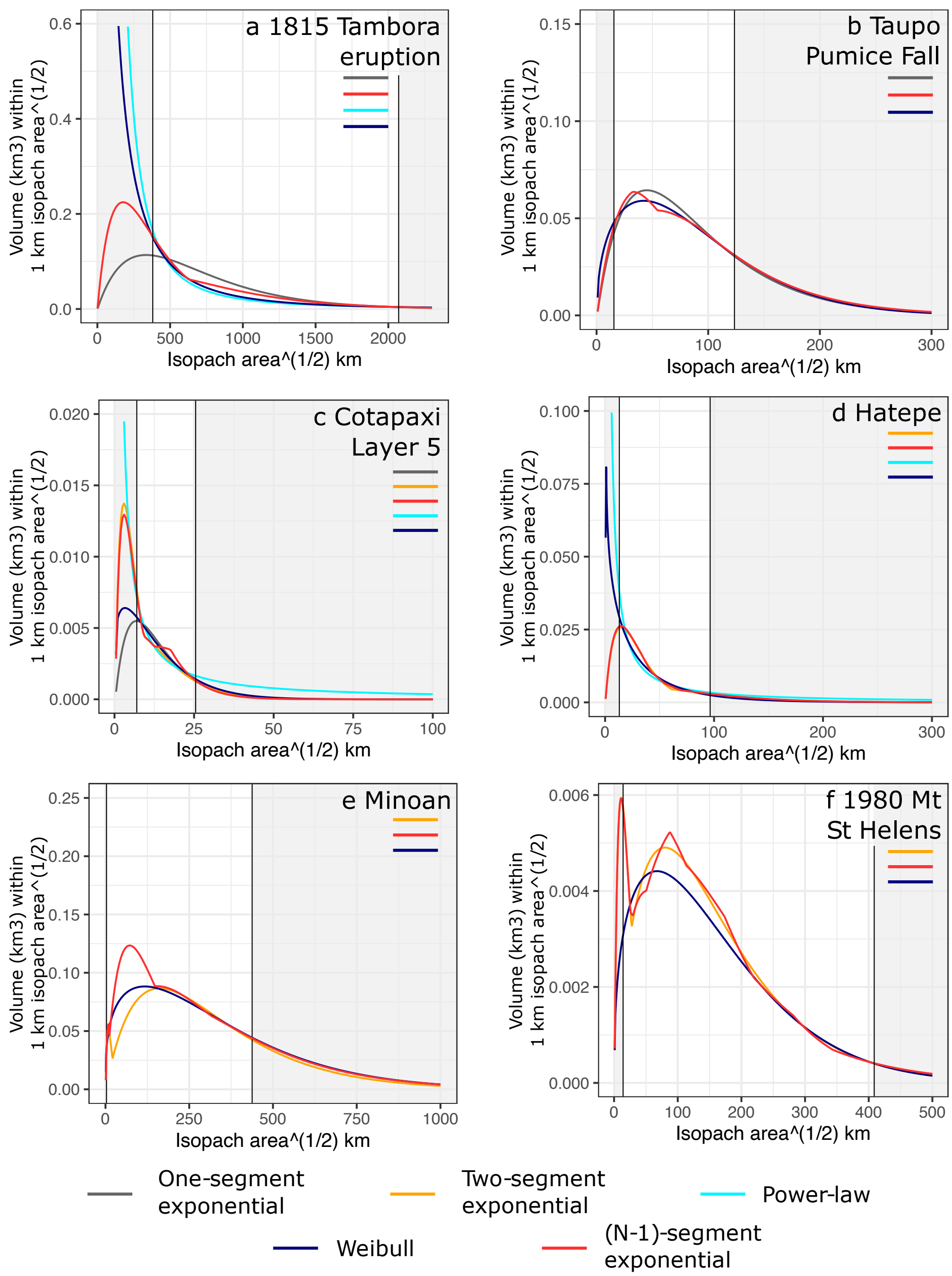

Figure 4: How tephra volume is distributed with $\sqrt{\text{isopach area}}$ for the six tephra datasets based on the fitted curves calculated based on Eq. 5. Gray areas correspond to extrapolated volumes. The proximal extrapolated volume in e (the Minoan tephra) is too small to be plotted as the thickest isopach has an area of 9 km^2.

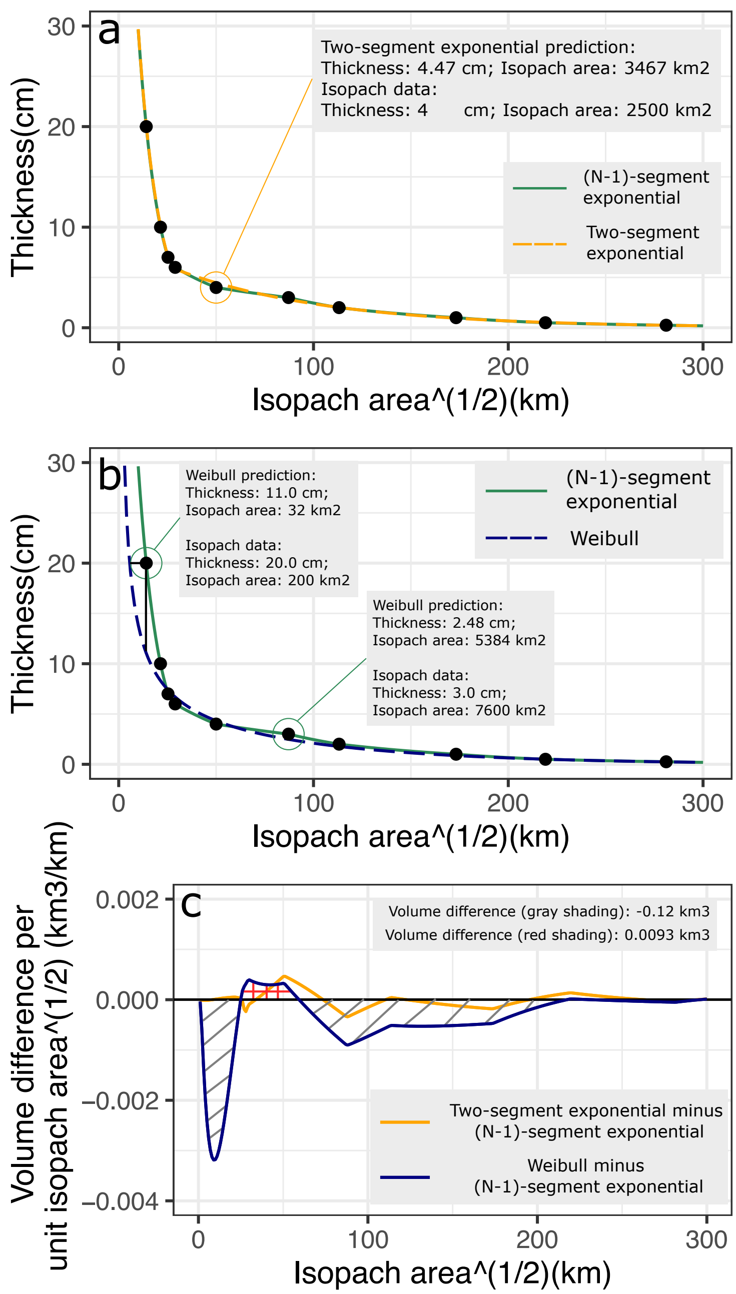

Figure 5: a and b: fitted two- and (N-1)-segment exponential, and Weibull curves compared pairwise. Note that the y-axis shows the non-logged thickness. Selected thickness and isopach area predictions from the curves are labeled; c: the volume per $\sqrt{\text{isopach area}}$ difference between the two- and (N-1)-segment exponential curves (yellow line) and between the Weibull and (N-1)-segment exponential curves (dark blue line). The volumes that the shaded areas correspond to are marked.

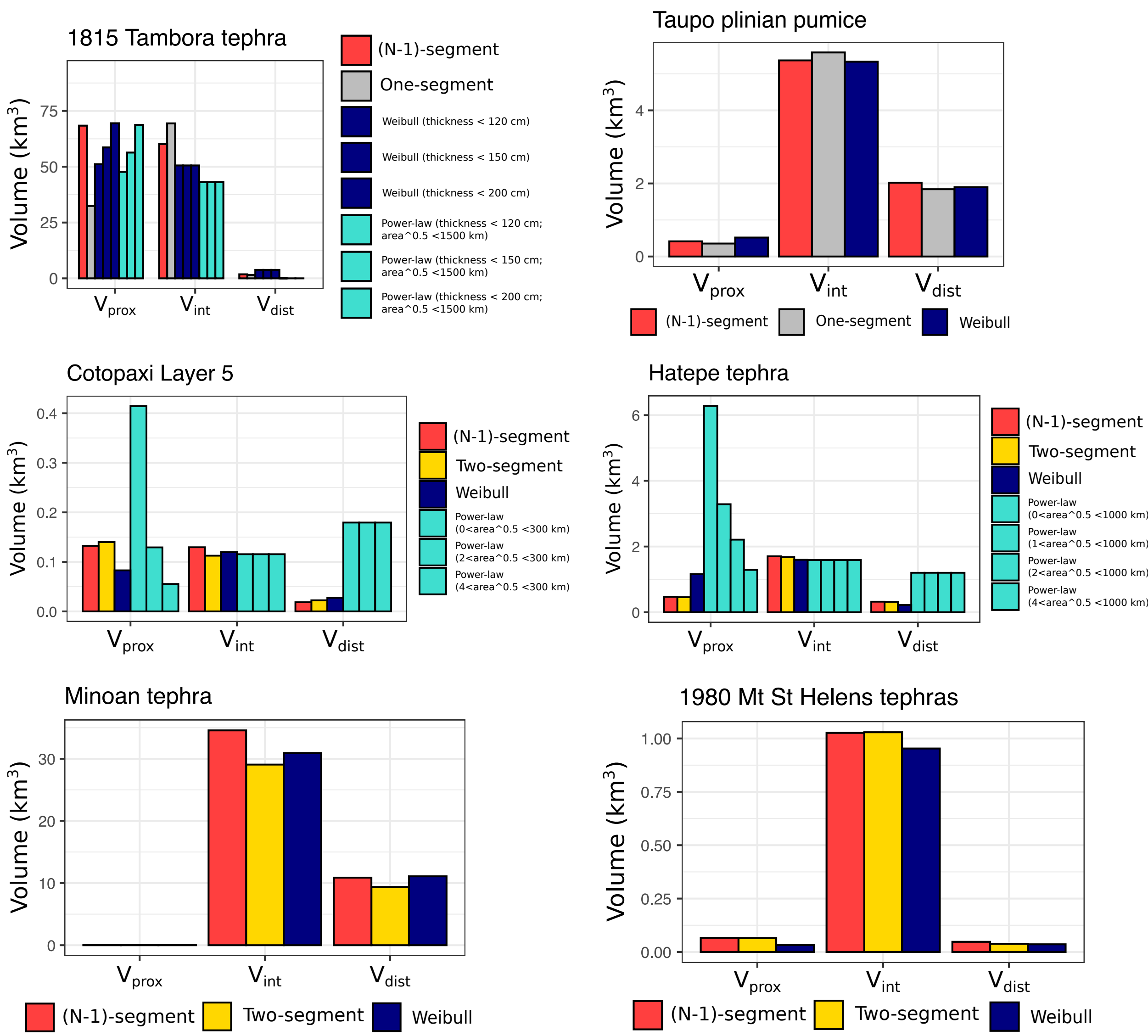

Figure 6: V_{prox}, V_{int}, and V_{dist} estimated from different fitted curves for the six tephra datasets shown as histograms with integration limits given.

8 Acknowledgments

Q. Yang and S.F. Jenkins were partly supported by the National Research Foundation Singapore and the Singapore Ministry of Education under the Research Centres of Excellence initiative (Project Number: NRF2018NRF-NSFC003ES-010). This work comprises Earth Observatory of Singapore contribution number 473, and forms part of a jointly funded collaboration (NRF-NSFC) between Q. Yang and S.F. Jenkins at the Asian School of the Environment/Earth Observatory of Singapore at NTU and H. Wei, J. Xu, and B. Pan at the Chinese Earthquake Administration. We appreciate the comments and suggestions from C. Bonadonna and S. Biass, which greatly improved the organization and quality of the manuscript.

References

S. Biass and C. Bonadonna. A quantitative uncertainty assessment of eruptive parameters derived from tephra deposits: the example of two large eruptions of cotopaxi volcano, ecuador. *Bulletin of Volcanology*, 73(1):73–90, 2011.

S. Biass, C. Bonadonna, and B. F. Houghton. A step-by-step evaluation of empirical methods to quantify eruption source parameters from tephra-fall deposits. *Journal of Applied Volcanology*, 8(1):1–16, 2019.

S. Biasse, G. Bagheri, W. Aeberhard, and C. Bonadonna. Terror: towards a better quantification of the uncertainty propagated during the characterization of tephra deposits. *Statistics in Volcanology*, 1(2): 1–27, 2014.

C. Bonadonna and A. Costa. Estimating the volume of tephra deposits: a new simple strategy. *Geology*, 40 (5):415–418, 2012.

C. Bonadonna and B. Houghton. Total grain-size distribution and volume of tephra-fall deposits. *Bulletin of Volcanology*, 67(5):441–456, 2005.

C. Bonadonna, G. Ernst, and R. Sparks. Thickness variations and volume estimates of tephra fall deposits: the importance of particle reynolds number. *Journal of Volcanology and Geothermal Research*, 81(3-4): 173–187, 1998.

H. M. Buckland, K. V. Cashman, S. L. Engwell, and A. C. Rust. Sources of uncertainty in the mazama isopachs and the implications for interpreting distal tephra deposits from large magnitude eruptions. *Bulletin of Volcanology*, 82(3):1–17, 2020.

M. Bursik, R. Sparks, J. Gilbert, and S. Carey. Sedimentation of tephra by volcanic plumes: I. theory and its comparison with a study of the fogo a plinian deposit, sao miguel (azores). *Bulletin of Volcanology*, 54 (4):329–344, 1992.

S. Carey and R. Sparks. Quantitative models of the fallout and dispersal of tephra from volcanic eruption columns. *Bulletin of volcanology*, 48(2):109–125, 1986.

R. Constantinescu, A. Hopulele-Gligor, C. B. Connor, C. Bonadonna, L. J. Connor, J. M. Lindsay, S. Charbonnier, and A. C. Volentik. The radius of the umbrella cloud helps characterize large explosive volcanic eruptions. *Communications Earth & Environment*, 2(1):1–8, 2021.

R. Constantinescu, J. White, C. Connor, A. Hopulele-Gligor, S. Charbonnier, J.-C. Thouret, J. Lindsay, and D. Bertin. Uncertainty quantification of eruption source parameters estimated from tephra fall deposits. *Geophysical Research Letters*, 49(6):e2021GL097425, 2022.

M. L. Daggitt, T. A. Mather, D. M. Pyle, and S. Page. Ashcalc–a new tool for the comparison of the exponential, power-law and weibull models of tephra deposition. *Journal of Applied Volcanology*, 3(1):1–8, 2014.

S. Engwell, R. Sparks, and W. Aspinall. Quantifying uncertainties in the measurement of tephra fall thickness. *Journal of Applied Volcanology*, 2(1):1–12, 2013.

S. Engwell, W. Aspinall, and R. Sparks. An objective method for the production of isopach maps and implications for the estimation of tephra deposit volumes and their uncertainties. *Bulletin of volcanology*, 77(7):1–18, 2015.

J. Fierstein and M. Nathenson. Another look at the calculation of fallout tephra volumes. *Bulletin of volcanology*, 54(2):156–167, 1992.

R. M. Green, M. S. Bebbington, G. Jones, S. J. Cronin, and M. B. Turner. Estimation of tephra volumes from sparse and incompletely observed deposit thicknesses. *Bulletin of Volcanology*, 78(4):25, 2016.

J. Kandlbauer and R. Sparks. New estimates of the 1815 tambora eruption volume. *Journal of Volcanology and Geothermal Research*, 286:93–100, 2014.

E. Kawabata, M. S. Bebbington, S. J. Cronin, and T. Wang. Modeling thickness variability in tephra deposition. *Bulletin of volcanology*, 75(8):1–14, 2013.

M. Klawonn, B. F. Houghton, D. A. Swanson, S. A. Fagents, P. Wessel, and C. J. Wolfe. Constraining explosive volcanism: subjective choices during estimates of eruption magnitude. *Bulletin of Volcanology*, 76(2):1–6, 2014a.

M. Klawonn, B. F. Houghton, D. A. Swanson, S. A. Fagents, P. Wessel, and C. J. Wolfe. From field data to volumes: constraining uncertainties in pyroclastic eruption parameters. *Bulletin of Volcanology*, 76(7): 1–16, 2014b.

T. Koyaguchi and M. Ohno. Reconstruction of eruption column dynamics on the basis of grain size of tephra fall deposits: 1. methods. *Journal of Geophysical Research: Solid Earth*, 106(B4):6499–6512, 2001.

F. Legros. Minimum volume of a tephra fallout deposit estimated from a single isopach. *Journal of Volcanology and Geothermal Research*, 96(1-2):25–32, 2000.

F. Maeno, M. Nagai, S. Nakada, R. E. Burden, S. Engwell, Y. Suzuki, and T. Kaneko. Constraining tephra dispersion and deposition from three subplinian explosions in 2011 at shinmoedake volcano, kyushu, japan. *Bulletin of Volcanology*, 76(6):1–16, 2014.

L. G. Mastin, M. Guffanti, R. Servranckx, P. Webley, S. Barsotti, K. Dean, A. Durant, J. W. Ewert, A. Neri, W. I. Rose, et al. A multidisciplinary effort to assign realistic source parameters to models of volcanic ash-cloud transport and dispersion during eruptions. *Journal of Volcanology and Geothermal Research*, 186(1-2):10–21, 2009.

C. G. Newhall and S. Self. The volcanic explosivity index (vei) an estimate of explosive magnitude for historical volcanism. *Journal of Geophysical Research: Oceans*, 87(C2):1231–1238, 1982.

J.-M. Prival, J.-C. Thouret, S. Japura, L. Gurioli, C. Bonadonna, J. Mariño, and K. Cueva. New insights into eruption source parameters of the 1600 ce huaynaputina plinian eruption, peru. *Bulletin of Volcanology*, 82(1):1–19, 2020.

D. M. Pyle. The thickness, volume and grainsize of tephra fall deposits. *Bulletin of Volcanology*, 51(1):1–15, 1989.

D. M. Pyle. New estimates for the volume of the minoan eruption. *Thera and the Aegean world III*, 2: 113–121, 1990.

D. M. Pyle. Sizes of volcanic eruptions. In *The encyclopedia of volcanoes*, pages 257–264. Elsevier, 2015.

J. Rougier, R. Sparks, W. Aspinall, and S. Mahony. Estimating tephra fall volume from point-referenced thickness measurements. *Geophysical Journal International*, 230(3):1699–1710, 2022.

A. M. Sarna-Wojcicki, S. Shipley, R. B. Waitt Jr, D. Dzurisin, and S. H. Wood. Areal distribution, thickness, mass, volume, and grain size of air-fall ash from the six major eruptions of 1980. 1981.

R. Sulpizio. Three empirical methods for the calculation of distal volume of tephra-fall deposits. *Journal of volcanology and geothermal research*, 145(3-4):315–336, 2005.

S. Takarada and H. Hoshizumi. Distribution and eruptive volume of aso-4 pyroclastic density current and tephra fall deposits, japan: a m8 super-eruption. *Frontiers in Earth Science*, 8:170, 2020.

G. Walker. The waimihia and hatepe plinian deposits from the rhyolitic taupo volcanic centre. *New Zealand journal of geology and geophysics*, 24(3):305–324, 1981.

G. P. Walker. The taupo pumice: product of the most powerful known (ultraplinian) eruption? *Journal of volcanology and geothermal research*, 8(1):69–94, 1980.

G. P. L. Walker and R. Croasdale. Two plinian-type eruptions in the azores. *Journal of the Geological Society*, 127(1):17–55, 1971.

J. White, C. B. Connor, L. Connor, and T. Hasenaka. Efficient inversion and uncertainty quantification of a tephra fallout model. *Journal of Geophysical Research: Solid Earth*, 122(1):281–294, 2017.

G. T. Williams, S. F. Jenkins, S. Biass, H. E. Wibowo, and A. Harijoko. Remotely assessing tephra fall building damage and vulnerability: Kelud volcano, indonesia. *Journal of Applied Volcanology*, 9(1):1–18, 2020.

Q. Yang and M. Bursik. A new interpolation method to model thickness, isopachs, extent, and volume of tephra fall deposits. *Bulletin of Volcanology*, 78(10):1–21, 2016.

Q. Yang, E. B. Pitman, M. Bursik, and S. F. Jenkins. Tephra deposit inversion by coupling tephra2 with the metropolis-hastings algorithm: algorithm introduction and demonstration with synthetic datasets. *Journal of Applied Volcanology*, 10(1):1–24, 2021.